COMPARISON OF METHODS FOR TRAJECTORY TRACKING FOR REDUNDANT ROBOT MANIPULATORS UNDER HOLONOMIC SCLERONOMIC CONSTRAINTS

Felipe F. Cardoso*, Fernando Lizarralde†

*PETROBRAS - Petróleo Brasileiro S.A., Rio de Janeiro/RJ, Brasil

†Programa de Engenharia Elétrica - COPPE, Universidade Federal do Rio de Janeiro, Brasil

Emails: `felipefc@petrobras.com.br, fernando@coep.ufrj.br`

Abstract— This paper presents a comparison of two methods used for trajectory tracking: kinematic control and optimization problem via sequential quadratic programming. The end-effector of a redundant serial robot manipulator has to track a desired trajectory while a point of the kinematic chain is subject to a holonomic scleronomic constraint. In addition two manipulability indices are take into account, the first refers to the Jacobian before the constraint and the second refers to the constrained Jacobian. Experiments are performed in a Baxter® robot.

Keywords— manipulability, trajectory tracking, holonomic constraint.

Resumo— Este artigo apresenta uma comparação entre dois métodos usados para rastreamento de trajetória: controle cinemático e problema de otimização via programação quadrática sequencial. O efetuador de um manipulador robótico serial redundante deve seguir a trajetória desejada enquanto um ponto em sua cadeia está sujeito a uma restrição escleronômica holonômica. Adicionalmente dois índices de manupulabilidade são levados em conta, o primeiro se refere ao Jacobiano antes da restrição e o segundo se refere ao Jacobiano restrito. Experimentos são realizados em um robo Baxter®.

Palavras-chave— manipulabilidade, rastreamento de trajetória, restrição holonômica.

1 Introduction

An open chain robot is kinematically redundant if the number of joints is larger than the dimension of the task space (Murray et al., 1994). This provides the robot with an increased level of dexterity that may be used to avoid singularities, joint limits, and workspace obstacles, but also to minimize joint torque, energy or, in general, to optimize suitable performance indices.

In many situations the environment adds constraints that can be overcomed by redundant robots, in these situations robots need to satisfy these constraints while performing tasks. Examples can be found in:

- Minimally invasive surgery (From, 2013; Coutinho, 2015): At the insertion point in the body's patient during a minimally invasive surgery the surgery instrument should not move transversely in order to not cause serious lesions in the epithelium.
- Extreme environment (Hosford, 2016): The robot performs the main task in a poorly mapped environment.
- Mapping (Everist and Shen, 2009): Mapping opaque single path tubes through insertion.
- Manipulation of Valves (Faria et al., 2015): Optimal control to avoid joint limits closing valves.

In robotics manipulation a singularity is a configuration where the behavior of a manipulator cannot be predicted so the physical measures quantities (as example the forces) become infinite or non deterministic. The manipulability measure is a index given by the product of the singular values of the Jacobian matrix.

It can be noted that during singular configurations the determinant of the matrix Jacobian is null. This means null singular values and also a null manipulability. So a manipulability analysis could help to improve a control strategy when redundant robots are subject to constraints because it is an indication of how close the manipulator is from a singular configuration.

A general discussion about manipulability for robot manipulators can be found in (Siciliano et al., 2009). Manipulability of constrained systems is discussed in (Wen and Wilfinger, 1999) and for constrained serial manipulators in (From et al., 2014). A geometrical approach can be found in (Park and Kim, 1998; Wen and O'Brien, 2003). A control scheme based on the constrained Jacobian in task space for constrained manipulators is discussed in (Pham et al., 2014; Coutinho, 2015). In industrial applications a confined environment can be seen as a kinematic constraint in the manipulator chain (Simas et al., 2013; Everist and Shen, 2009). In (Yoshikawa, 1985) is presented a method for maximize the manipulability for a non-constrained redundant manipulator using the null space of the geometric Jacobian. In (Zhang et al., 2012) an optimization problem is proposed in order to maximize the manipulability of self-motion planning in a redundant manipulator. In (Dufour and Suleiman, 2017) the inverse kinematics problem is solved as a optimization problem maximizing the manipulability index.

This work presents a general formulation to determine the Jacobian of a serial redundant manipulator with constraints in a point of this kinematic chain, the called constrained Jacobian. As stated by (From et al., 2014) the analysis of manipulability of a serial redundant constrained manipulator must take into account not only the constrained Jacobian, but also the manipulator Jacobian until the joint before the constraint. So a multi-objective problem is presented in order to maximize two manipulability indices (corresponding to constrained Jacobian and the Jacobian until the joint before the constraint) while the end-effector follows a trajectory and the imposed constraints are satisfied. The analysis is addressed to an arm of the Baxter® robot with seven revolute joints and a plane constraint. Experiments results are presented and compared between two methods, a analytic approach for kinematic control in Cartesian space and multi-objective optimization problem via sequential quadratic programming.

The following notation and definitions are used throughout the paper. $\mathbb{R} := (-\infty, \infty)$ and $\mathbb{R}^+ := [0, \infty)$. A frame is represented by F, F_i is the i-th frame. The joint angle vector is represented by θ, the i-th joint angle is θ_i, a joint angle vector $\theta_{i,j} = [\theta_i \ \theta_{i+1} \ \cdots \ \theta_{j-1} \ \theta_j]$. Given $x \in \mathbb{R}^3$, $[x]$ is the skew symmetric matrix. The linear and angular velocities are denoted by $v \in \mathbb{R}^3$ and $\omega \in \mathbb{R}^3$, respectively. The velocity at a frame i is defined by:

$$V_i = \begin{bmatrix} v_i \\ \omega_i \end{bmatrix}.$$

The adjoint matrix $\Phi_{i,j}$ (Siciliano et al., 2009) maps velocities between F_i and F_j:

$$V_{i+1} = \Phi_{i+1,i} V_i,$$

$$\Phi_{i+1,i} = \begin{bmatrix} R^T_{i,i+1} & -R^T_{i,i+1}[(r_{i,i+1})_i] \\ 0 & R^T_{i,i+1} \end{bmatrix},$$

where $R_{i,i+1} \in SO(3)$ is the orientation of F_{i+1} with respect to F_i and $(r_{i,i+1})_i$ is the vector between frames F_i and F_{i+1} represented in F_i. The superscripts B and G mean that a variable is defined in the body frame and inertial frame, respectively.

The geometric Jacobian in body coordinates is defined by (Siciliano et al., 2009):

$$V_i^B = J_i^B(\theta_{1,i})\dot{\theta}_{1,i},$$

$$J_i^B(\theta_{1,i}) = \begin{bmatrix} (h_1)_i \times (r_{1,i})_i & \cdots & (h_{i-1})_i \times (r_{i-1,i})_i & 0 \\ (h_1)_i & \cdots & (h_{i-1})_i & (h_i)_i \end{bmatrix}$$

where $(h_j)_i$ is the axis of rotation of the joint j in F_i (without loss of generality, here, only revolute joints are considered). For a Jacobian matrix J, $J^T(JJ^T)^{-1}$ is the pseudo-inverse denoted by $J^\dagger$.

The pose of the manipulator is represented by $p(\theta) \in \mathbb{R}^b$ while the desired pose is $p_d \in \mathbb{R}^b$, b is the task space dimension.

2 Constraints in Applied Mechanics

A constraint is defined as the mathematical expression of restriction in motion of particles or rigid bodies. In a system with n particles $P_i(i = 1, 2, ..., n)$ in the space $\mathbb{S}$, the position of this particles is defined by $r_i^G = \begin{bmatrix} x_i & y_i & z_i \end{bmatrix}^T$.

Considering two points $P_1(x_1, y_1, z_1) \in \mathbb{R}^3$ and $P_2(x_2, y_2, z_2) \in \mathbb{R}^3$, the distance between P_1 and P_2 is:

$$r_{1,2}^G = |r_1^G - r_2^G|. \tag{1}$$

If (1) is invariant to a translation then $\mathbb{S}$ is homogeneous. If (1) is invariant to a rotation then $\mathbb{S}$ is isotropic (Jazar, 2011).

The motion of the system in time t is a trajectory of configuration points ($S_C point$) in a space defined as the configuration space, $S_C space$: $X_C = \{x_i, y_i, z_i : i = 1, 2, ..., a\}$ (a is the number of particles of the system). The $S_C space$ is homogeneous and isotropic.

2.1 Holonomic Constraint

A holonomic constraint is a equation in function of configuration displacement and/or time. A scleronomic holonomic constraint is defined in configuration space:

$$f(\theta_1, \theta_2, \theta_3, ..., \theta_N) = f(\theta) = 0. \tag{2}$$

In (2) θ_i is a system variable and θ is the vector of system variables, considering a manipulator with only revolute joints θ is the joint angle vector.

When a scleronomic holonomic constraint is imposed in a finite displacement, there is too a constraint in a infinitesimal displacements $d\theta_i$:

$$df(\theta, t) = f_1(d\theta, dt) = 0. \tag{3}$$

A scleronomic constraint for infinitesimal displacements is defined by:

$$\sum_{i=1}^{N} \frac{\partial f}{\partial \theta_i} d\theta_i = 0, \tag{4}$$

The differential constraints in (4) is total differential and can be integrated in (2), so it is a scleronomic holonomic constraint.

2.2 Generalized Coordinates

The configuration degrees of freedom f_C is defined by:

$$f_C = N - L, \tag{5}$$

where N is the system degrees of freedom and L the number of independent holonomic constraints.

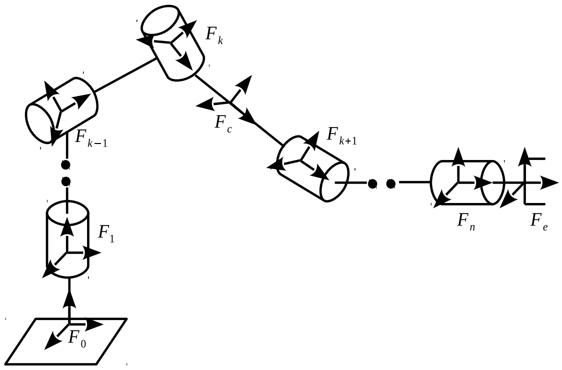

Figure 1: Serial manipulator with revolute joints.

Each holonomic constraint defines a subspace in X_C that a $S_C point$ can move. Thus $d\theta$ has f_C degrees of freedom and a new set of variables of size f_C can be defined to determine the N components of $d\theta$. These variables are the generalized coordinates:

$$g = g_i(\theta_1, \theta_2, ..., \theta_N) \quad i = 1, 2, ..., fc. \tag{6}$$

3 Constrained Jacobian

The constrained Jacobian is a matrix that maps velocities of joint space in task space that also take into account the holonomic constraints in the manipulator chain. A general formulation to obtain the constrained Jacobian of a constrained serial manipulator with one or more holonomic constraints located in only one point in this chain is presented below.

In Figure 1 a system with n joints (only revolute joints are considered) is presented. F_0 is inertial frame, the frame F_i $(i = 1, ..., n)$ is tied to the i-th joint, F_e is the end-effector frame, F_k is the frame in the joint before the holonomic constraints and F_c the frame at the holonomic constraints.

The velocity at F_k in the body frame and the joint velocity are related by:

$$V_k^B = J_k^B(\theta_{1,k})\dot{\theta}_{1,k}. \tag{7}$$

The velocity at F_c and F_k are related by:

$$V_c^B = \Phi_{c,k} V_k^B. \tag{8}$$

Suppose that a point $\in \mathbb{R}^b$ in the kinematic chain of the manipulator is subject to a holonomic constraint where the point belongs to a surface $\mathbb{S}$. So a scleronomic holonomic constraint in $S_C space$ (recalling that the system variables vector is the joint angle vector) at F_c can be defined using a matrix $H \in \mathbb{R}^{m\times 6}$ where m is the dimension of the constraint, i.e.,

$$H V_c^B = 0. \tag{9}$$

Substituting (7) and (8) in (9), one has

$$H \Phi_{c,k} J_k^B(\theta_{1,k})\dot{\theta}_{1,k} = 0. \tag{10}$$

Defining

$$\wedge = H \Phi_{c,k}, \tag{11}$$

the joint velocity vector satisfying (10) is given by:

$$\dot{\theta}_{1,k} = J_k^{B\dagger}(\theta_{1,k}) \wedge^{\#} u_f, \tag{12}$$

where $\wedge^{\#}$ spans the null space of $\wedge$ and u_f is a control degree of freedom. Using (5) the dimension of u_f (b_{u_f}) is defined for $N = k$ (manipulator degrees of freedom until the holonomic constraints) and $L = m$ (number of independent holonomic constraints considering that all lines of H are linearly independent):

$$b_{u_f} = k - m. \tag{13}$$

The end-effector velocity is given by:

$$V_e^B = J_e^B(\theta)\dot{\theta}. \tag{14}$$

Separating $J_e^B(\theta)$ into two parts, the end-effector velocity can be written as:

$$V_e^B = \begin{bmatrix} J_{e1}^B(\theta) & J_{e2}^B(\theta_{k+1,n}) \end{bmatrix} \begin{bmatrix} \dot{\theta}_{1,k} \\ \dot{\theta}_{k+1,n} \end{bmatrix}. \tag{15}$$

Replacing (12) in (15) creates:

$$V_e^B = \begin{bmatrix} J_{e1}^B(\theta) J_k^{B\dagger}(\theta_{1,k}) \wedge^{\#} & J_{e2}^B(\theta_{k+1,n}) \end{bmatrix} \begin{bmatrix} u_f \\ \dot{\theta}_{k+1,n} \end{bmatrix}. \tag{16}$$

In (16) the product of matrix multiplication $J_{e1}^B(\theta) J_k^{B\dagger}(\theta_{1,k})$ only depends of $\theta_{k+1,n}$ in the condition that $J_k^B(\theta_{1,k})$ is not singular (see (Coutinho, 2015) for proof). Thus $J_r^B(\theta_{k+1,n})$, called constrained Jacobian matrix, is defined:

$$J_r^B(\theta_{k+1,n}) = \begin{bmatrix} J_{e1}^B(\theta) J_k^{B\dagger}(\theta_{1,k}) \wedge^{\#} & J_{e2}^B(\theta_{k+1,n}) \end{bmatrix}. \tag{17}$$

Then rewriting (16) with (17):

$$V_e^B = J_r^B(\theta_{k+1,n}) \begin{bmatrix} u_f \\ \dot{\theta}_{k+1,n} \end{bmatrix}. \tag{18}$$

4 Manipulability Indices

The manipulability is an index that represents the manipulator distance to singular configurations. For a given Jacobian matrix $J(\theta)$ the manipulability measure is:

$$w = \sqrt{det(J(\theta) J^T(\theta))}. \tag{19}$$

In order to analyze the manipulability of a constrained serial manipulator two Jacobian matrices have to be taken into account, the geometric Jacobian until the joint before the constraint $J_k^B(\theta_{1,k})$ and the constrained Jacobian $J_r^B(\theta_{k+1,n})$.

The manipulability of $J_k^B(\theta_{1,k})$ is a measure of how efficiently the constrained manipulator can generate motions in F_k in order to track the desired trajectory of the end-effector:

$$w_k = \sqrt{det(J_k^B(\theta_{1,k}) J_k^{B^T}(\theta_{1,k}))}. \quad (20)$$

For the constrained Jacobian matrix $J_r^B(\theta_{k+1,n})$, which can only depends on the constraint type and kinematics of the joints after the constraint, the manipulability indicates the possibility of generating the desired trajectory in the end-effector associated with the use of u_f and $\dot{\theta}_{k+1,n}$:

$$w_r = \sqrt{det(J_r^B(\theta_{k+1,n}) J_r^{B^T}(\theta_{k+1,n}))}. \quad (21)$$

5 Kinematic Control in Cartesian Space

In this section a approach for kinematic control in Cartesian Space is presented, this scheme have been used in (Pham et al., 2014; Coutinho et al., 2014; Coutinho, 2015). Considering only the position in Cartesian space the end-effector position p_e must track a desired time-varying trajectory $p_d(t)$, so in the ideal case $p_e \rightarrow p_d(t)$, while a point in the manipulator chain is subject to one or more holonomic constraints.

The Figure 2 shows a block diagram for a kinematic position control loop in Cartesian space. The block Internal Control Loop is a robot internal controller that makes $\dot{\theta} = \dot{\theta}_d$. Utilizing the constrained position Jacobian $J_{rp}(\theta_{k+1,n}) \in \mathbb{R}^{3 \times n-m}$ that is equal to the first three lines of $J_r(\theta_{k+1,n})$, is possible to obtain the linear velocity of the end-effector $v_e \in \mathbb{R}^3$ from (18):

$$v_e = J_{rp}^B(\theta)\dot{\theta} = J_{rp}^B(\theta_{k+1,n}) \begin{bmatrix} u_f \\ \dot{\theta}_{n+1,k} \end{bmatrix}. \quad (22)$$

Still in Figure 2 integrating $\dot{\theta}$ over time and applying the forward kinematics results in p_e. The position error e_p is:

$$e_p = p_d - p_e. \quad (23)$$

For a Cartesian control signal $u_p = K_p e_p + \dot{p}_d(t)$, where $K_p \in \mathbb{R}^{3 \times 3}$ and u_p is a proportional plus feed forward controller, using (22) the constrained velocity vector $\begin{bmatrix} u_f & \dot{\theta}_{k+1,n} \end{bmatrix}^T \in \mathbb{R}^{n-m}$ is given by:

$$\begin{bmatrix} u_f \\ \dot{\theta}_{k+1,n} \end{bmatrix} = J_{rp}^{B^\dagger}(\theta_{k+1,n}) u_p. \quad (24)$$

Now $\dot{\theta}_{1,k}$ is obtained using $u_f \in \mathbb{R}^{k-m}$ from (24), $J_{kp}(\theta_{1,k}) \in \mathbb{R}^{3 \times k}$ is equal to the first three lines of $J_k(\theta_{1,k})$:

$$\dot{\theta}_{1,k} = J_{kp}^{B^\dagger}(\theta_{1,k}) \wedge^{\#} u_f. \quad (25)$$

$\dot{\theta}_d$ is the vertical concatenation of $\dot{\theta}_{1,k}$ from (24) and $\dot{\theta}_{k+1,n}$ from (25), $\dot{\theta}_d = \begin{bmatrix} \dot{\theta}_{1,k} & \dot{\theta}_{k+1,n} \end{bmatrix}^T$, so it can be rewritten in a matrix multiplication form using the terms of right side of equalities (24) and (25):

$$\dot{\theta}_d = \begin{bmatrix} J_{kp}^{B^\dagger}(\theta_{1,k})\wedge^{\#} & 0_{k,n-k} \\ 0_{n-k,k-m} & I_{n-k} \end{bmatrix} J_{rp}^{B^\dagger}(\theta_{k+1,n}) u_p. \quad (26)$$

In (22) v_e also can be rewritten in a matrix multiplication form because from (25) $u_f = (J_{kp}^{B^\dagger}(\theta_{1,k})\wedge^{\#})^\dagger \dot{\theta}_{1,k}$, so:

$$v_e = J_{rp}^B(\theta_{k+1,n}) \begin{bmatrix} J_{kp}^{B^\dagger}(\theta_{1,k})\wedge^{\#} & 0_{k,n-k} \\ 0_{n-k,k-m} & I_{n-k} \end{bmatrix}^\dagger \dot{\theta}. \quad (27)$$

Now in order to obtain the position error dynamics, derives (23), substitutes $\dot{p}_d(t)$ with $u_p - K_p e_p$ and considering that $\dot{\theta} = \dot{\theta}_d$ substituting (26) in (27) implies $v_e = u_p$:

$$\dot{e}_p = \dot{p}_d - v_e = u_p - K_p e_p - v_e = -K_p e_p \quad (28)$$

where with a positive definite matrix K_p implies that $\lim_{t \to \infty} e_p(t) = 0$.

There are two manipulability indices, w_k and w_r, the control strategy in this Section, that is applied in (Pham et al., 2014; Coutinho et al., 2014), does not address specifically those two indices (or any other that can be defined), it only strives to follow a trajectory with the holonomic constraints satisfied. So a modification of (24) and (25) is proposed, it consists in expand the null space of $J_{rp}^B(\theta_{k+1,n})$ and $J_{kp}^B(\theta_{1,k})$ rewriting (24) and (25) respectively as:

$$\begin{aligned} \begin{bmatrix} u_f \\ \dot{\theta}_{k+1,n} \end{bmatrix} &= J_{rp}^{B^\dagger}(\theta_{k+1,n}) u_p + \\ (I_{n-k} - J_{rp}^{B^\dagger}&(\theta_{k+1,n}) J_{rp}^B(\theta_{k+1,n}))\mu_r, \end{aligned} \quad (29)$$

$$\begin{aligned} \dot{\theta}_{1,k} &= J_{kp}^{B^\dagger}(\theta_{1,k}) \wedge^{\#} u_f + \\ (I_k - J_{kp}^{B^\dagger}&(\theta_{1,k}) J_{kp}^B(\theta_{1,k}))\mu_k, \end{aligned} \quad (30)$$

where μ_k and μ_r are additional degrees of freedom that are utilized for maximize a function, in this case the manipulabilities defined in (20) and (21). So:

$$\mu_k = K_k \left(\frac{\partial w_k(\theta_{1,k})}{\partial \theta} \right), \quad (31)$$

$$\mu_k = K_r \left(\frac{\partial w_r(\theta_{k+1,n})}{\partial \theta} \right), \quad (32)$$

where $K_k \in \mathbb{R}^+$ and $K_r \in \mathbb{R}^+$ define the weight of (31) and (32) respectively.

6 Multi-objective Problem Formulation

In this section a multi-objective problem is proposed, the manipulator must follow the trajectory while maintaining the manipulability indices

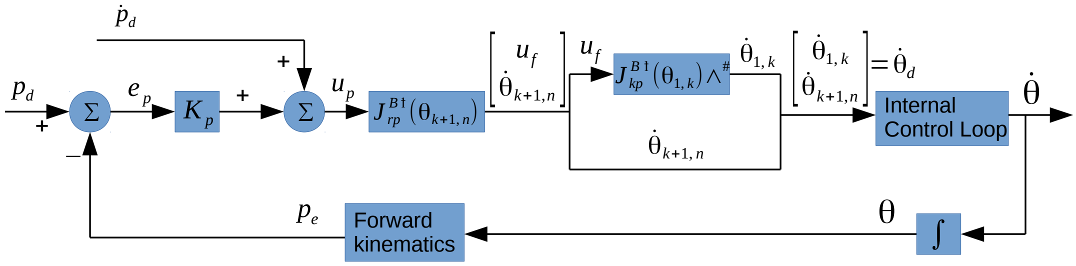

Figure 2: Kinematic position control loop.

as high as possible and satisfying the holonomic constraints.

Whenever a manipulator tracks a trajectory the position error in end-effector at an instant t is the difference between the desired position $p_d(t)$ and the actual position $p_e(\theta(t))$:

$$e(t) = p_d(t) - p_e(\theta(t)). \tag{33}$$

Using a method that finds a solution $\dot{\theta}^s(t)$, a joint velocity command for the manipulator at a fixed step time T, that aims to bring the position error in (33) to zero in a step time, the predicted error is:

$$\tilde{e}(t+T) = p_d(t+T) - p_e(\tilde{\theta}(t+T)), \tag{34}$$

where the predicted joint angle vector in (34) is

$$\tilde{\theta}(t+T) = \theta(t) + \dot{\theta}^s(t)T. \tag{35}$$

In a optimization problem a function can be maximized searching through the minimization of his negative. Then functions f_1 and f_2 are respectively the negative of w_k and w_r evaluated at the predicted joint angle vector in (35):

$$f_1 = -\sqrt{det(J^B_{kp}(\tilde{\theta}_{1,k}(t+T))J^{B\,T}_{kp}(\tilde{\theta}_{1,k}(t+T)))}, \tag{36}$$

$$f_2 = -\sqrt{det(J^B_{rp}(\tilde{\theta}_{k+1,n}(t+T))J^{B\,T}_{rp}(\tilde{\theta}_{k+1,n}(t+T)))}. \tag{37}$$

As a multi-objective problem, a linear scalarization is used for functions f_1 and f_2 together with a parameter $\alpha \in \mathbb{R}^+$ where $0 \leq \alpha \leq 1$. For a serial redundant manipulator with one or more holonomic constraints in a point of this chain and subject to track a trajectory, using (36) and (37) a multi-objective problem (the solution is the joint velocity vector $\dot{\theta}^s(t)$) is defined as:

$$\min \quad \alpha f_1 + (1-\alpha) f_2, \tag{38}$$

$$\text{s.t.} \quad -\delta \leq \tilde{e}(t+T) \leq \delta \tag{39}$$

$$H\Phi_{c,k} J^B_{kp}(\tilde{\theta}_{1,k}(t+T))\dot{\theta}^s_{1,k}(t) = 0, \tag{40}$$

$$\theta^- \leq \tilde{\theta}(t+T) \leq \theta^+, \tag{41}$$

$$\dot{\theta}^- \leq \dot{\theta}^s(t) \leq \dot{\theta}^+, \tag{42}$$

where $\delta \in \mathbb{R}^+$ is a constant, θ^+ and θ^- denote respectively the upper and lower joint angle limits while $\dot{\theta}^+$ and $\dot{\theta}^-$ denote respectively the upper and lower joint velocity limits.

The decision variables of the multi-objective problem in (38) to (42) are the joint velocities $\dot{\theta}_i$. Although the decision variables are not explicit in (38), (39) and (41) the relations are defined in (34) to (37). The search method for multi-objective problem in (38) to (42) could be any algorithm that solves nonlinear convex optimization problems. In this work a sequential quadratic programming (sqp) algorithm is used.

The objective function in (38) is minimized at each step of the sqp method reflecting in a momentary value for w_k and w_r. The inequality in (39) means that the predicted error is between a lower and a upper bound. The constraint (40), same expression of (10) but now evaluated at $\tilde{\theta}(t+T)$ and $\dot{\theta}^s(t)$, is the scleronomic holonomic constraint in the manipulator chain. The inequality constraints (41) and (42) are the manipulator physical constraints in terms of joint angle limits and joint velocity limits respectively.

In order to gather the values of w_k or w_r at each step of the sqp method in one index, the integral of the manipulability indices are taken into account:

$$W_k = \int_0^{t_f} w_k dt, \tag{43}$$

$$W_r = \int_0^{t_f} w_r dt, \tag{44}$$

where t_f is the time that the trajectory tracking ends. So one solution s^* is defined as a pair W_k and W_r for a fixed α.

Remark 1 *The problem (38) to (42) can be treated as a mono-objective but would result in a single solution where the α parameter would have to be fixed a priori. This unique solution results in manipulability values that might not be good compared to other attainable values. In fact, there may be a range of α values that make the indices cooperative an another range of α values the where*

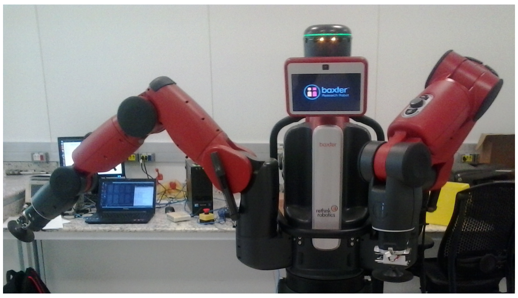

Figure 3: Baxter® robot used in experiments.

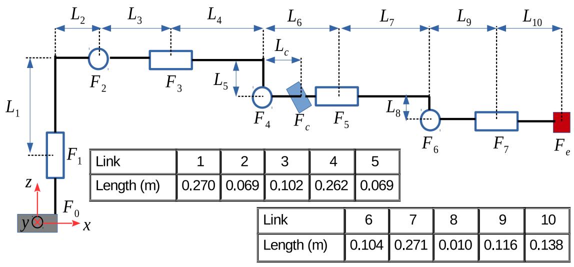

Figure 4: Kinematic model of Baxter's right arm with plane constraint between F_4 and F_5.

Table 1: Parameters of Baxter's right arm.

Joint	θ_i *(angle limit (rad))*	$\dot{\theta}_i$ *(velocity limit (rad/s))*
1	θ_1 (-1.70 to 1.70)	$\dot{\theta}_1$ (-2.0 to 2.0)
2	θ_2 (-2.14 to 1.04)	$\dot{\theta}_2$ (-2.0 to 2.0)
3	θ_3 (-3.02 to 3.02)	$\dot{\theta}_3$ (-2.0 to 2.0)
4	θ_4 (-0.05 to 2.61)	$\dot{\theta}_4$ (-4.0 to 4.0)
5	θ_5 (-3.05 to 3.05)	$\dot{\theta}_5$ (-4.0 to 4.0)
6	θ_6 (-1.57 to 2.09)	$\dot{\theta}_6$ (-4.0 to 4.0)
7	θ_7 (-3.05 to 3.05)	$\dot{\theta}_7$ (-4.0 to 4.0)

the indices are in opposition. Then only with the multi-objective problem is possible to verify the correlation between the indices of manipulability, this correlation changes according to the location and type of constraint.

7 Experiments

In this section two trajectory tracking experiments are presented using the right arm of the Baxter® robot, Figure 3. The objective is track the desired trajectory (only position of the end-effector is considered) while maintaining the manipulability indices as high as possible using the approach for kinematic control in Cartesian space and the multi-objective formulation problem.

The Table 1 specifies the joint limits (angles and velocities) for the Baxter's right arm. In order to restrict the search space in the sqp method the limits of joint velocities are set for $-0.5\ rad/s$ to $0.5\ rad/s$ for all $\dot{\theta}_i$, this is necessary to avoid that $\dot{\theta}^s(t)$ go to the lower and upper physical velocity limits in consecutive steps of the sqp method.

A scleronomic holonomic constraint in a point of Baxter kinematic chain between F_4 and F_5 (F_i is tied to the i-th joint) defined by the displacement $L_c = 50\ mm$ can be seen in Figure 4. In Figure 4 there is a plane constraint in F_c meaning there is no movement on one axis, in this particular case the x axis on the frame F_c. So the dimension of the constraint is the set $\mathbb{R}$ and the equation of the scleronomic holonomic constraint in (11) has the following vector:

$$H = \begin{bmatrix} 1 & 0 & 0 & 0 & 0 & 0 \end{bmatrix}. \qquad (45)$$

The constraint in Figure 4 is after F_4 and before F_5 so $k = 4$. Figure 5 shows w_k (considering only the position Jacobian $J^B_{4p}(\theta_{1,4})$) as function of

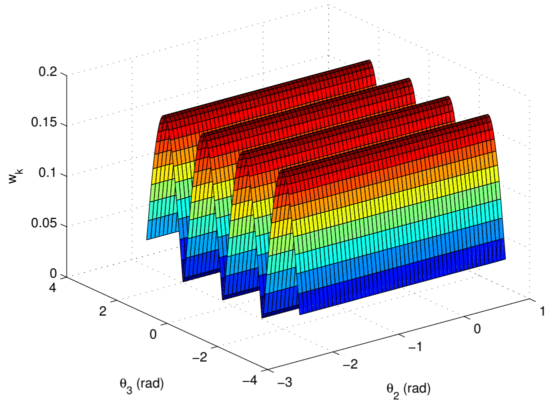

Figure 5: Manipulability w_k with $k = 4$, w_k is multiplied by 10^3.

θ_2 and θ_3. As $J^B_{4p}(\theta_{1,4})$ takes into account only position until F_4, w_k does not depend on θ_4 neither θ_1 because in the inertial frame the last column of $J_{4p}(\theta_{1,4})$ is null (no θ_4) while in the body frame the first column is null (no θ_1), the manipulability value is not affected for frame changes. The singular configuration is reached when $\theta_3 = 0$ as also multiple of $\theta_3 = \pm\pi/2$. The variation of θ_2 does not effect w_k. High values of w_k are reached near odd multiples of $\theta_3 = \pm\pi/4$.

Figure 6 shows w_r (considering only the position Jacobian $J^B_{rp}(\theta_{5,7})$) in function of θ_5 and θ_6. As θ_7 is tied to a revolute joint in x axis it does not change the end-effector position (only orientation) so it does not change the index w_r. Visualization of angle values for singular configurations would be tricky in a 3D plot so Figure 6 shows w_r in a 2D plot, a dark blue area means the manipulator is near a singular configuration while a dark red area means the manipulability reached a high value.

The end-effector position is represented by a three element vector in the following order, position in axes x, y and z ($p_x(\theta(t))$, $p_y(\theta(t))$ and $p_z(\theta(t))$ respectively) that can be found by the

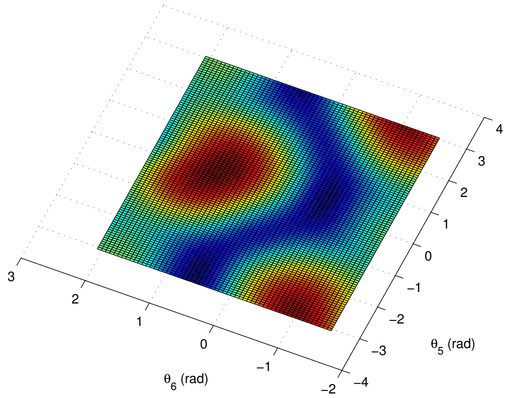

Figure 6: Manipulability w_r in a $\theta_5 - \theta_6$ space with plane constraint between frames F_4 and F_5.

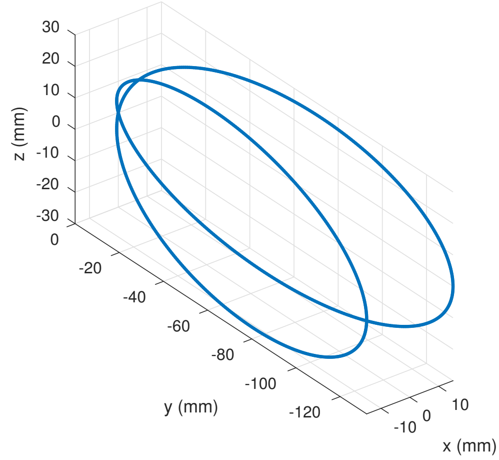

Figure 7: Desired trajectory for case I.

Table 2: Gains.

Experiment	K_k	K_r
1	0	0
2	1	0
3	0	0.3
4	5	0.5

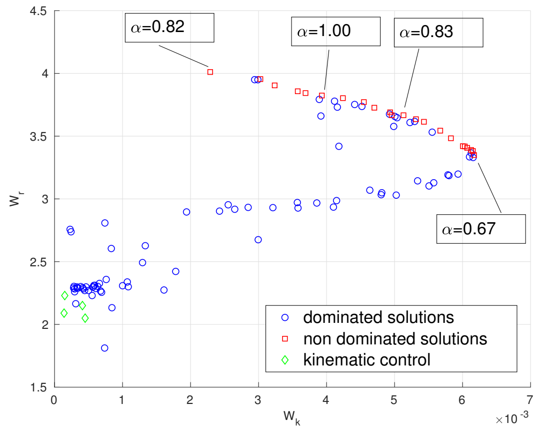

Figure 8: W_k and W_r for case I.

forward kinematics:

$$p_e(\theta) = \begin{bmatrix} p_x(\theta) \\ p_y(\theta) \\ p_z(\theta) \end{bmatrix}. \quad (46)$$

The first wave of experiments consists in applying the kinematic control, scheme of Figure 2, with the following matrix $K_p = diag(2.5, 3, 3.75)$ where $diag$ is the diagonal matrix.

The gains K_k an K_r are defined in Table 2. Increasing K_r beyond 0.5 leads the system to instability and increasing K_k does not change significantly the manipulability indices. One solution is a pair W_k and W_r for a line in Table 2.

In the second wave of experiments the multi-objective problem formulation from Section 6 is used. Using the sqp method a set of solutions s^* is generated for $\alpha = \begin{bmatrix} 0 & 0.01 & \cdots & 0.99 & 1 \end{bmatrix}$. In this case one solution is a pair W_k and W_r for a fixed α, that way this set has 101 solution classified in dominated and non dominated (a solution is non dominated if does not exist another solution equal or better in all objectives at same time).

In the first trajectory the end-effector of the constrained manipulator must track the following desired trajectory:

$$p_d(t) = \begin{bmatrix} p_x(0) + 15\sin(\omega t) \\ p_y(0) + 66\cos(2\omega t) - 66 \\ p_z(0) + 30\sin(2\omega t) \end{bmatrix} mm, \quad (47)$$

where $p_x(0)$, $p_y(0)$ and $p_z(0)$ are respectively the initial positions in axes x, y and z and $\omega = 2\pi/40 \ rad/s$ is the frequency. A sketch of the desired smooth trajectory is in Figure 7 considering the origin as initial point. The joint angle initial state is $\theta(0) = \begin{bmatrix} 0 & -\pi/6 & \pi/2 & \pi/4 & -\pi/3 & \pi/4 & 0 \end{bmatrix}^T rad$, the initial position is $p_x(0) = 960 \ mm$, $p_y(0) = -426 \ mm$ and $p_z(0) = 595 \ mm$, the task duration is 40 s.

The solution plot is in Figure 8, for the 101 multi-objective problem solutions 22 are non dominated (color red) and 79 are dominated (color blue). The Figure 8 still shows the indices W_k and W_r for 4 experiments of kinematic control, these 4 solutions (color green) are clearly dominated. Some values of α that form the global Pareto-optimal set are explicit in Figure 8, so it can be noted that the Pareto set is made by solutions with a high value of α.

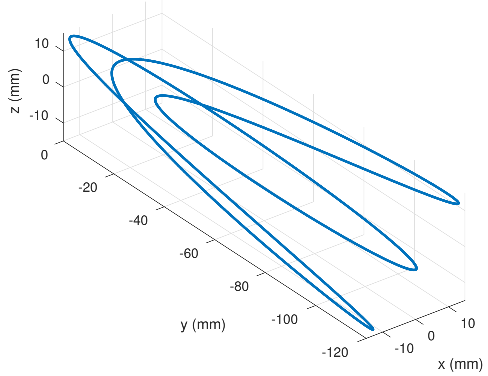

Figure 9: Desired trajectory for case II.

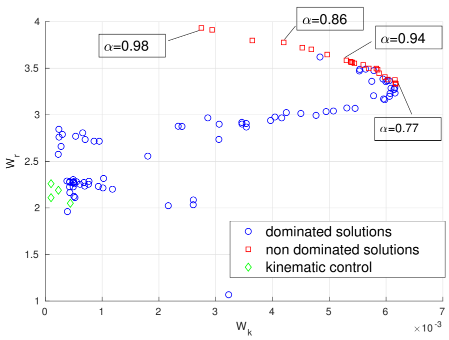

Figure 10: W_k and W_r for case II.

7.1 Case II

In the second trajectory the desired trajectory is:

$$p_d(t) = \begin{bmatrix} p_x(0) + 15\sin(\omega t) \\ p_y(0) + 66\cos(2\omega t) - 66 \\ p_z(0) + 30\sin(2\omega t) \end{bmatrix} mm, \quad (48)$$

where ω, $\theta(0)$ and task duration are the same from the first trajectory. A sketch of the desired trajectory with edges is in Figure 9.

The solution plot is in Figure 10, for the 101 multi-objective problem solutions again 22 are non dominated (color red), 79 are dominated (color blue) and the solutions of kinematic control (color green) are clearly dominated. The values of α that form the global Pareto-optimal, as can be seen in Figure 10, again are high.

8 Conclusions

The multi-objective problem formulation was successful in achieving high levels of manipulability in both trajectories. That is, manipulability reaches the peaks of Figures 5 or 6 according to alpha.

The proposed kinematic control failed in maintain the system stability for a increase of K_r, so it could not achieve a high level of manipulability in Figures 5 and 6. Further investigation should be made to determine the causes and correct the instability of the system. Other goal is add another method for comparison, the optimization problem via quadratic programming.

Acknowledgment

This work was supported in part by CNPq and PETROBRAS, Brazil.

References

Coutinho, F. G. (2015). Controle de manipulador redundante com restrições cinemáticas aplicado a cirurgias robóticas assistidas, *Programa de Engenharia Elétrica, Universidade Federal do Rio de Janeiro* .

Coutinho, F. G., Pham, C. D., From, P. J. and Lizarralde, F. (2014). Abordagem analítica para controle no espaço operacional de manipuladores com restrições cinemáticas, *XX Congresso Brasileiro de Automática* pp. 958–964.

Dufour, K. and Suleiman, W. (2017). On integrating manipulability index into inverse kinematics solver, *IEEE/RSJ International Conference on Intelligent Robot and Systems* pp. 6967–6972.

Everist, J. and Shen, W. (2009). Mapping opaque and confined environments using proprioception, *IEEE International Conference on Robotics and Automation* pp. 1041–1046.

Faria, R., Kucharczak, F., Freitas, G., Leite, A., Lizarralde, F., Galassi, M. and From, P. (2015). A methodology for autonomous robotic manipulation of valves using visual sensing, *IFAC Workshop on Automatic Control in Offshore Oil and Gas Production* pp. 227–234.

From, P. J. (2013). On the kinematics of robotic-assisted minimally invasive surgery, *Modeling, Identification and Control, 34, pp 69-82* .

From, P. J., Robertsson, A. and Johansson, R. (2014). On the manipulability of velocity-constrained serial robotic manipulators, *In World Congress* (1): 10934–10939.

Hosford, L. A. (2016). Development and testing of an impedance controller on an anthropomorphic robot for extreme environment operations, *Department of Mechanical Engineering, Massachusetts Institute of Technology* .

Jazar, R. N. (2011). Advanced dynamics: Rigid body multibody and aerospace applications, *Wiley* .

Murray, R. M., Li, Z. and Sastry, S. S. (1994). A mathematical introduction to robotic manipulation, *CRC Press* .

Park, F. C. and Kim, J. W. (1998). Manipulability and singularity analysis of multiple robot systems: A geometric approach, *IEEE International Conference on Robotics and Automation* pp. 1032–1037.

Pham, C. D., Coutinho, F., Lizarralde, F., Hsu, L. and From, P. J. (2014). An analytical approach to operational space control of robotic manipulators with kinematic constraints, *In World Congress* **19**(1): 8509–8515.

Siciliano, B., Sciavicco, L., Villani, L. and Oriolo, G. (2009). Robotics modelling, planning and control, *Springer* .

Simas, H., Dias, A., Martins, D. and Pieri, E. R. D. (2013). Analytical equation for motion constraints in confined environments for a p6r redundant robot, *22nd International Congress of Mechanical Engineering* pp. 4425–4435.

Wen, J. T. and O'Brien, F. (2003). Singularities in three-legged platform-type parallel mechanisms, *IEEE Transactions on Robotics and Automation* **19**(4): 720–726.

Wen, J. T. and Wilfinger, L. S. (1999). Kinematic manipulability of general constrained rigid multibody systems, *IEEE Transactions on Robotics and Automation* **15**(3): 558–567.

Yoshikawa, T. (1985). Manipulability of robot mechanisms, *The Int. J. Robot. Res* **4**(2): 3–9.

Zhang, Y., Guo, D., Li, K. and Li, J. (2012). Manipulability-maximizing self-motion planning and control of redundant manipulators with experimental validation, *IEEE International Conference on Mechatronics and Automation* pp. 1829–1834.